

Dissociative Water Potential for Molecular Dynamics Simulations

T. S. Mahadevan and S. H. Garofalini*

Interfacial Molecular Science Laboratory, Department of Materials Science and Engineering, Rutgers University, Piscataway, New Jersey 08855

Received: March 31, 2007; In Final Form: May 16, 2007

A new interatomic potential for dissociative water was developed for use in molecular dynamics simulations. The simulations use a multibody potential, with both pair and three-body terms, and the Wolf summation method for the long-range Coulomb interactions. A major feature in the potential is the change in the short-range O–H repulsive interaction as a function of temperature and/or pressure in order to reproduce the density–temperature curve between 273 K and 373 K at 1 atm, as well as high-pressure data at various temperatures. Using only the change in this one parameter, the simulations also reproduce room-temperature properties of water, such as the structure, cohesive energy, diffusion constant, and vibrational spectrum, as well as the liquid–vapor coexistence curve. Although the water molecules could dissociate, no dissociation is observed at room temperature. However, behavior of the hydronium ion was studied by introduction of an extra H⁺ into a cluster of water molecules. Both Eigen and Zundel configurations, as well as more complex configurations, are observed in the migration of the hydronium.

Introduction

Simulation and understanding of water has been an ongoing issue for over three decades, and its importance cannot be overstated. While many water potentials exist,^{1–18} most are nondissociating, being either rigid or, at most, flexible. Because of the large number of papers regarding simulations of water, the reader is referred to a couple of excellent reviews currently available.^{19,20} In general, the properties of water can be expressed fairly accurately over a narrow range of temperatures and pressures. One major problem has been the failure of these potentials to reproduce the density versus temperature curve over the liquid-state range from 273 to 373 K.¹³ Even in cases where the temperature of maximum density is well reproduced, the potentials often fail at reproducing the rest of the density–temperature curve.¹⁸ Since our major interest is in the behavior of water interacting with silica and silica pores and the atomistic evaluation of the anomalous expansion of confined water, the exact reproduction of the bulk liquid expansion becomes paramount. A new nondissociative water potential recently developed reproduces the molecular state, liquid water, and the liquid–vapor coexistence curve extremely well.²¹ However, we also want to include the dissociation of water onto the silica surface, similar to earlier simulations of water on silica,²² but with a more accurate water potential. Other dissociative water potentials exist but are similarly not sufficiently accurate with respect to the liquid equation of state.^{10,23} To obtain a more appropriate water potential, we modified the rigid water potential developed by Guillot and Guissani (GG)¹⁵ so that it more accurately reproduced the features of bulk water, but also allowed for dissociation.

Dissociation also allows for the study of the hydronium ion, although the quantum nature of the proton makes a classical approach only approximate. The hydronium ion has been previously modeled classically,²⁴ with reasonable results. Two important structural models for the hydronium ion in water are the Zundel²⁵ complex, H₅O₂⁺, with the H₃O⁺ ion H-bonded to

a normal H₂O molecule, and the Eigen²⁶ complex, H₉O₄⁺, with the H₃O⁺ ion H-bonded to three water molecules. Recent ab initio path integral simulations showed that these two structures are limiting cases of more complex behavior.²⁷

We first describe the details of the potential function and modifications that were required, followed by the properties of the simulated water.

Computational Procedure

The new dissociative water potential is a multibody potential with both two-body and three-body terms. The pair term is based on the rigid water potential developed earlier (GG).¹⁵ However, in our potential, intramolecular interactions are added. Also, because of the use of the Wolf summation to account for the long-range nature of the Coulomb term, parameters in the original GG potential were modified. The potential is given as

$$U_{2\text{-body}} = U_{qq} + U_{q^d q^d} + U_{qq^d} + U_{q^d q} + U_{\text{rep}} + U_{\text{disp}} \quad (1)$$

where

$$U_{qq}(r_{ij}) = \frac{q_i q_j}{r_{ij}} \operatorname{erfc}\left(\frac{r_{ij}}{\beta}\right) \quad (2)$$

$$U_{q^d q^d}(r_{ij}) = \frac{q_i^d q_j^d}{r_{ij}} \operatorname{erf}\left(\frac{r_{ij}}{2\xi_{ij}}\right) \operatorname{erfc}\left(\frac{r_{ij}}{\beta}\right) \quad (3)$$

$$U_{qq^d}(r_{ij}) = \frac{q_i q_j^d}{r_{ij}} \operatorname{erf}\left(\frac{r_{ij}}{\sqrt{2}\xi_{ij}}\right) \operatorname{erfc}\left(\frac{r_{ij}}{\beta}\right) \quad (4)$$

$$U_{q_i q_j}(r_{ij}) = \frac{q_i^d q_j}{r_{ij}} \operatorname{erf}\left(\frac{r_{ij}}{\sqrt{2}\xi_{ij}}\right) \operatorname{erfc}\left(\frac{r_{ij}}{\beta}\right) \quad (5)$$

$$U_{\text{rep}}(r_{ij}) = A_{\text{rep}}^{ij} \frac{\operatorname{erfc}(z_{ij})}{z_{ij}} \left(z_{ij} = \frac{r_{ij}}{2\xi_r^{ij}}\right) \quad (6)$$

$$U_{\text{disp}}(r_{ij}) = \frac{-C_6^{ij}}{r_{ij}^6} \quad (7)$$

In the original GG potential, $q_i^d \sim -q_i/4$, so we made the constant relation $q_i = -4q_i^d$, using $q_{\text{H}}^d = -0.113$ and allowing O to be twice the H values.

For the long-range coulomb interactions, we use the Wolf summation²⁸ rather than the Ewald sum. The Wolf summation gives the coulomb energy contribution as

$$E^{\text{ele}} = E_{(1)}^{\text{ele}} + E_{(2)}^{\text{ele}} = \frac{1}{2} \sum_{i=1}^N \sum_{j \neq i=1}^{\infty} \frac{q_i q_j \operatorname{erfc}(r_{ij}/\beta)}{r_{ij}} + \frac{1}{2} \sum_{i=1}^N \sum_{j \neq i=1}^{\infty} \frac{q_i q_j \operatorname{erf}(r_{ij}/\beta)}{r_{ij}} \quad (8)$$

The second term can be shown to be negligible with the appropriate choice of β and cutoff distance R_c , giving the energy as the following:

$$E_{(1)}^{\text{ele}} = \frac{1}{2} \sum_{i=1}^N \sum_{\substack{j \neq i \\ r_{ij} < R_c}} \left(\frac{q_i q_j \operatorname{erfc}(r_{ij}/\beta)}{r_{ij}} - \lim_{r_{ij} \rightarrow R_c} \left\{ \frac{q_i q_j \operatorname{erfc}(r_{ij}/\beta)}{r_{ij}} \right\} \right) - \left(\frac{\operatorname{erfc}(R_c/\beta)}{2R_c} + \frac{1}{\beta\pi^{1/2}} \right) \sum_{i=1}^N q_i^2 \quad (9)$$

We have employed the Wolf summation in simulations of SiC²⁹ and variations of the Wolf summation have been applied to simulations of water.³⁰

In the original GG potential, the charge distribution on the each atom is modeled with a point charge on the atom plus a diffuse charge that reduces the net charge as a function of the distance from the atom based on the error function. The application of a diffuse charge distribution to a water potential has been previously discussed.³¹ A modified version of their potential has been elegantly applied to water in a recent paper,²¹ in which they also discuss the benefits of a diffuse charge model on achieving both high density and low density behavior. In the GG potential, the diffuse charge contributions to the total charge of an ion i varies as a function of the distance based on the q_i^d term, which is opposite in sign to the q_i term, thus reducing the effective charge on ion i as a function of the distance between an ij pair and the value of ξ . In the present case, the coulomb potential is also reduced by the long-range summation parameter β in the erfc term in eqs 2–5. The smaller the value of ξ , the more rapidly the contribution of the diffuse charge on the total charge increases to its maximum. In our case, ξ is set large so that the diffuse charges contribute only slightly to the total charge. However, this is offset by the erfc term of the Wolf summation in eqs 2–5. The pair potential acts between all pairs of atoms and does not distinguish between different molecules. This enables a uniform description for the interactions within and between molecules that depends only on the distance between the atoms. This results in a fully atomistic model of water that allows for dissociation. This

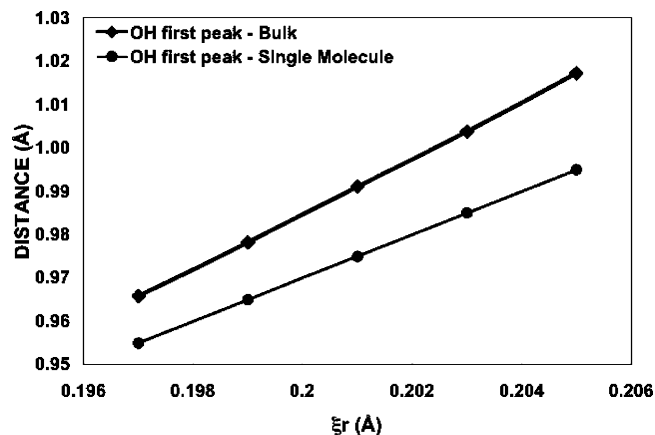


Figure 1. Variation in the OH distance in a single water molecule and within bulk water as a function of a term in the OH short-range repulsion, ξ_r .

TABLE 1: (a) Parameters of the Two-Body Potential; (b) Charges on Species; (c) Three-Body Parameters; (d) A Matrix of Equation 12 Columns A(:,0)–A(:,2); (e) A Matrix of Equation 12 Columns A(:,3)–A(:,5)

| (a) Parameters of the Two-Body Potential | | | | |
|---|------------------------------|-------------------------------|--------------|-----------------------------|
| species | A^{rep} (J) | ξ (Å) | ξ_r (Å) | C_6 (J Å ⁶) |
| O–H | 2.283×10^{-16} | 24 | $f(T,P)$ | |
| O–O | 4.250×10^{-17} | 24 | 0.610 | 4.226×10^{-18} |
| H–H | | 24 | | |
| (b) Charges on Species | | | | |
| species/multiple | q/e | q^d/e | | |
| O | −.904 | +226 | | |
| H | +452 | −.113 | | |
| (c) Three-Body Parameters | | | | |
| species | λ (ergs) | $r_{\alpha\beta}^0$ (Å) | γ (Å) | $\theta_{\text{HOH}}^\circ$ |
| H–O–H | 30×10^{-11} | 1.6 | 1.3 | 100 |
| (d) A Matrix of Equation 12 Columns A(:,0)–A(:,2) | | | | |
| 0.655726502 | $-1.04442689 \times 10^{-2}$ | $8.31892416 \times 10^{-5}$ | | |
| 3.403472×10^{-4} | -3.986929×10^{-6} | 1.742261×10^{-8} | | |
| -4.057853×10^{-8} | 4.677537×10^{-10} | $-2.007873 \times 10^{-12}$ | | |
| 1.657262×10^{-12} | $-1.838785 \times 10^{-14}$ | 7.549619×10^{-17} | | |
| (e) A Matrix of Equation 12 Columns A(:,3)–A(:,5) | | | | |
| $-3.07929142 \times 10^{-7}$ | $5.44770929 \times 10^{-10}$ | $-3.73609493 \times 10^{-13}$ | | |
| $-3.364186 \times 10^{-11}$ | 2.419996×10^{-14} | 0 | | |
| 3.800411×10^{-15} | $-2.672717 \times 10^{-18}$ | 0 | | |
| $-1.355453 \times 10^{-19}$ | 8.939302×10^{-23} | 0 | | |

also means that the dissociated species, $\text{OH}^{-\delta}$ and $\text{H}^{+\delta}$, retain their original charge contributions, q_i and q_i^d for each O and H ion.

Besides the above two-body potential, a three-body potential of the following functional form was also added to the overall interaction:

$$U_3(r_i, r_j, r_k) = \nu_3(r_{ij}, r_{ik}, \theta_{jik}) \quad (10)$$

where

$$\nu_3(r_{ij}, r_{jk}, \theta_{jik}) = \lambda_{jik} \exp[\gamma_{ij}/(r_{ij} - r_{ij}^0) + \gamma_{ik}/(r_{ik} - r_{ik}^0)][\cos(\theta_{jik}) - \cos(\theta_{jik}^0)]^2 \quad (11)$$

for $r_{ij} < r_{ij}^0$ and $r_{ik} < r_{ik}^0$, and it is equal to 0 otherwise. The terms $r_{ij}^0 = r_{ik}^0 = r_{\alpha\beta}^0$ as given in Table 1c.

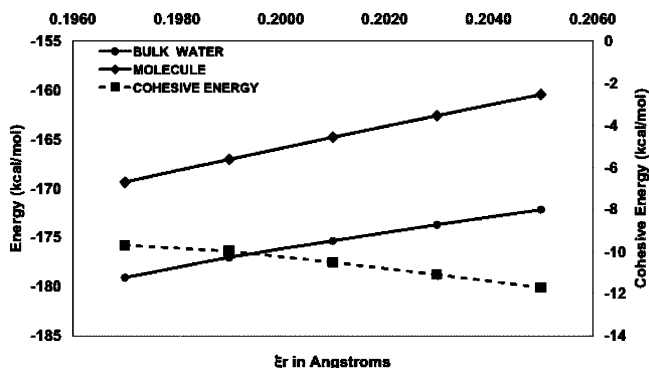


Figure 2. Variation in the energy in a single water molecule and bulk water as a function of the ξ_r term in the OH short-range repulsion (left axis) and the cohesive energy (right axis).

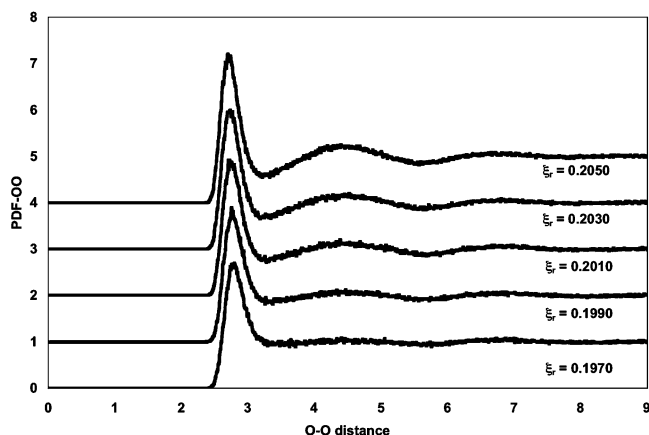


Figure 3. Variation in the OO pair distribution function (PDF) for bulk water as a function of the ξ_r term in the OH short-range repulsion.

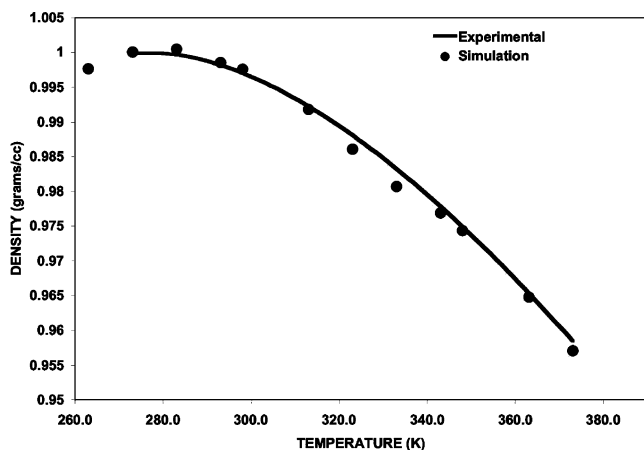


Figure 4. Result of optimizing the ξ_r term in the OH short-range repulsion on reproducing the density–temperature curve.

The effect of this function is to modify the interaction between three atoms depending on their deviation from the ideal angle, $\cos(\theta_{jik}^0)$. The use of such a function allows the water molecule to reach correct angles. The parameters used in the three-body potential are such that only the H–O–H angles in water are regulated to 104.2° (i.e., λ exists only for $jik = \text{HOH}$ and is identically zero for OOH or HHO or OHO). In order to achieve this angle, θ_{jik}^0 was set to 100° , which in combination with the H–H repulsive interaction created a minimum at 104° . The list of parameters finally selected are given in Table 1a–c.

The potentials were developed so that the simulated water matched the thermal expansion curve of water from 273 to 373

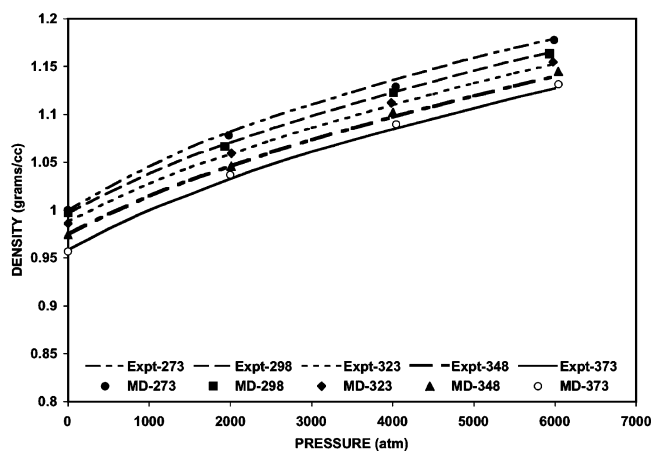


Figure 5. Result of optimizing the ξ_r term in the OH short-range repulsion on reproducing the density–pressure curve at four different temperatures.

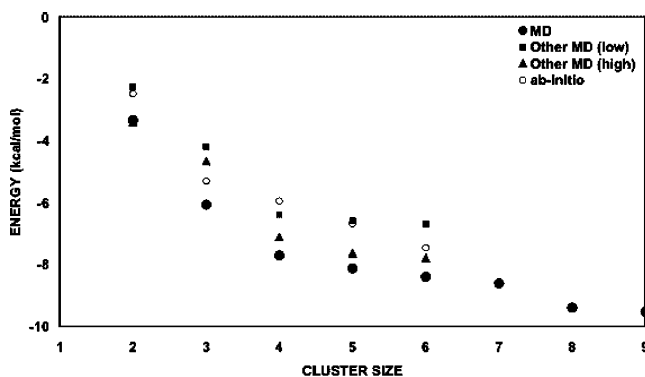


Figure 6. Cohesive energy per molecule of small water clusters at 1 K using finalized parameters given in Table 1 and the ξ_r term in the OH short-range repulsion obtained at 263 K. “MD” is the current data. Other data points come from ref 14, which contains data from other classical water potentials used in MD simulations (“other MD”) and ab initio calculations, with the lowest (low) and highest (high) cohesive energy per molecule from the other potentials (see text).

K³² (plus a data point at 263 K³³) and high-pressure data at several temperatures. Additional simulations of bulk water using the resultant potentials were used to generate the cohesive energy, structural data, vibrational spectra, liquid–vapor coexistence curve, and diffusion coefficients. In all of the simulations, the long-range Coulomb interactions were handled by the Wolf summation,²⁸ with a cutoff of 1 nm. System sizes less than 1 nm (individual molecule or small molecular clusters) were calculated using the full Coulomb interactions, without the Wolf summation. The time step was 0.1 fs in all simulations, and the simulations used a fifth-order Nordseick–Gear algorithm. *NPT* (constant number, pressure, temperature), *NVT* (constant number, volume, temperature) or *NVE* (constant number, volume, energy) ensembles were used.

Development of the Potential

In the current work, we modify the original GG potential¹⁵ in order to create a dissociative water potential that very accurately reproduces the density–temperature relation of the liquid while maintaining good structure, cohesive energy, and the diffusion coefficient. We do this by allowing the parameters to vary as a function of temperature and/or pressure. While many water models are able to accurately arrive at a reasonable structure and density near 298 K, most falter at reproducing the thermal expansion curve. In general, the observed trend in

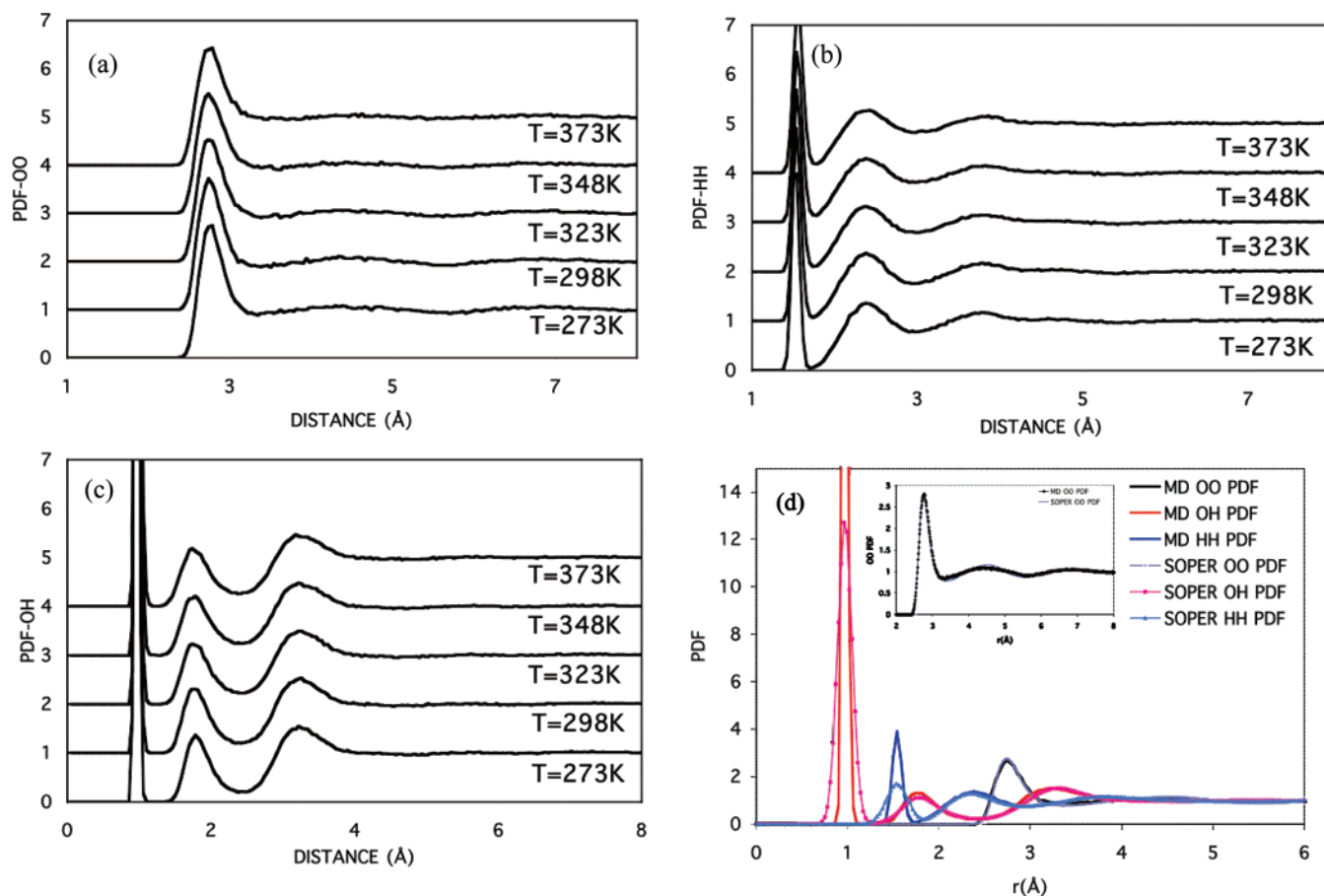


Figure 7. Pair distribution functions at different temperatures for (a) O–O, (b) H–H, and (c) O–H pairs. (d) Comparison between the MD simulations at 298 K and experimental data³⁵ for all three pairs, as well as a larger scale comparison of the OO PDF in the inset.

simulations has been that the density of water has been found to decrease at a greater rate with increase in temperature than experimental data.¹⁸

Previous studies have discussed the importance of the interactions at short distances on the accuracy of the interatomic potential.^{15,21} An effective way of making our water model better represent real water was achieved by allowing a change in a parameter with environment. In the current work, we have chosen to vary the short-range OH repulsive interaction via the ξ_r^{OH} parameter as a function of temperature and pressure.

The effect of this change in ξ_r^{OH} can be seen in properties of bulk water, and Figures 1, 2, and 3 are a simple demonstration of this and are not meant to be definitive. The effect of the change in ξ_r^{OH} on the OH distance is shown in Figure 1, and as a consequence of the above change in OH distance, the energy of bulk water also changes, as shown in Figure 2. The simulations were of a system of 392 water molecules in a box of approximate dimensions 2.3 nm \times 2.3 nm \times 2.3 nm. The *NPT* simulation was carried out at 1 atm of pressure and a constant temperature of 298 K for 200 000 timesteps. Structural and diffusion data were gathered over the final 100 000 timesteps. While this is a very short run time, these simulations were only designed to show the relative effect of ξ_r^{OH} on properties. Figure 2 shows the cohesive energy of bulk water and was obtained by calculating the difference between the average energy of a water molecule in bulk water and the average energy of a single gas-phase water molecule simulated with the same set of parameters. These energies may be different from those obtained in subsequent runs with final parameters and longer simulation times, but the trends are obvious. The

effect of ξ_r^{OH} on the OO pair distribution function (PDF) is shown in Figure 3. Small changes in ξ_r^{OH} cause changes in the OO PDF, especially the shape of the important second OO peak. Another consequence of changes in ξ_r^{OH} is the lowering in the self-diffusion coefficient at 298 K from 3.41×10^{-5} cm²/s to 1.08×10^{-5} cm²/s with increasing ξ_r^{OH} . Clearly, the short-range repulsion term, moderated by the ξ_r^{OH} term, plays an important role in the simulated properties. This effect can be controlled with various methods, such as added polarization terms, variable charge terms, etc. As shown here and below, we see the direct effect of the short-range term on properties.

In order to determine the correct values of ξ_r^{OH} that would enable the simulations to match experimental densities at various pressures (from 1 to 6000 atm) and various temperatures (from 263 to 373 K), a series of runs at each *T* and *P* were performed with various ξ_r^{OH} values, interpolating the value of ξ_r^{OH} to coincide with the experimental *T* and *P*. An initial molecular dynamics simulation of 392 water molecules in a periodic cubic simulation box of starting dimensions 2.175 nm \times 2.175 nm \times 2.486 nm was performed for 2.0×10^6 steps at 298 K in order to generate a starting water configuration for the subsequent runs to generate the final ξ_r^{OH} values. *NVE* conditions were used for the first 200 000 steps, with velocities scaled for the first 100 000 steps. The run was continued for another 1.8×10^6 steps under *NPT* conditions at 1 atm. Nominal parameters of $\xi_r^{\text{OH}} = 0.1989$ and $q_H^d = -0.113$ were used for this initial run. The final configuration of this run was used as the standard

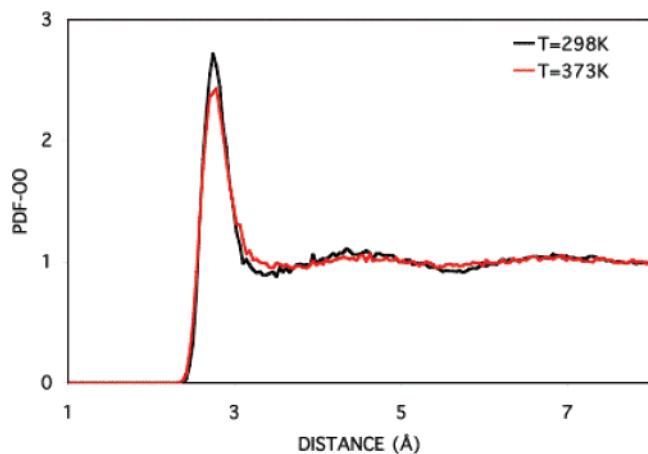


Figure 8. Comparison between the OO PDF at 298 and 373 K, showing the loss of structure at the elevated temperature in the decrease in the first peak maximum and an increase in the first minimum.

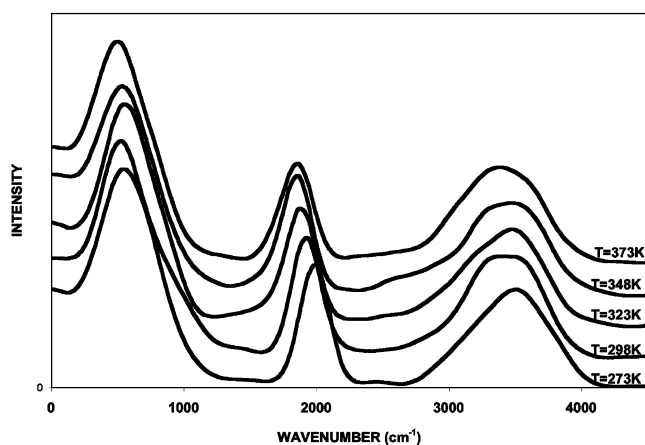


Figure 9. Vibrational frequency spectrum of simulated bulk water as a function of temperature.

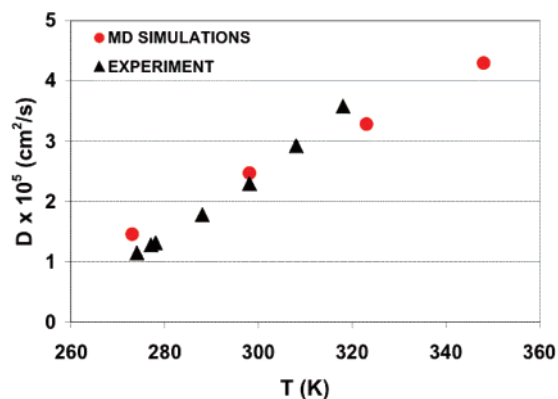


Figure 10. Diffusion coefficient, D (cm^2/s), as a function of temperature from the MD simulations versus experimental data (ref 36).

starting configuration for the additional NPT and NVE runs to determine the correct ξ_r^{OH} parameters for a particular T and P .

Each simulation that was then used to determine the correct ξ_r^{OH} values at each T and P was run for 1×10^6 steps. The densities averaged over every 2000 configurations were collected. The variation in densities over the entire run was around 2–3%, and the maximum variation was observed during the initial 15% of the moves. Thus for calculating the density of a particular simulation, the first 20% of the run was discarded and the average density for a particular temperature, pressure, and ξ_r^{OH} value was determined.

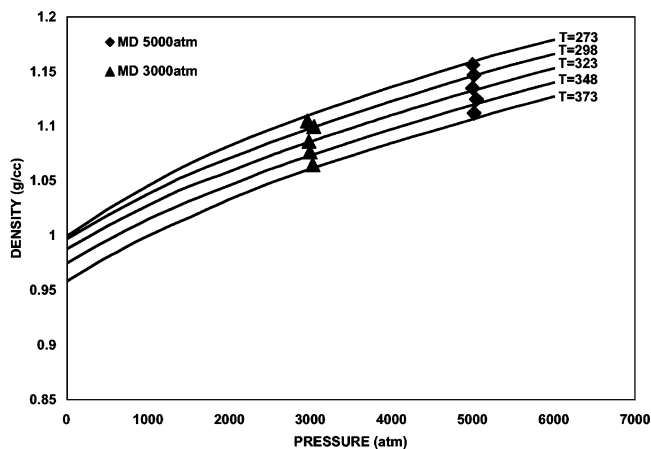


Figure 11. Density–pressure relation at 5000 and 3000 atm predicted from the simulations in comparison to the experimental data.

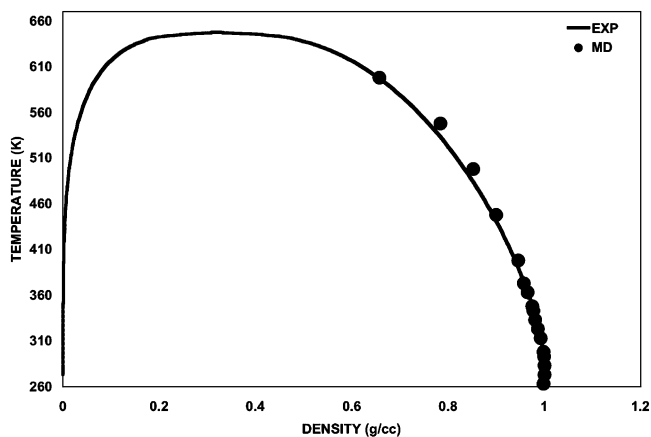


Figure 12. Liquid–vapor coexistence curve obtained from the simulations in comparison to experiment. The data at the four highest temperatures are predicted from the potential and functional form of ξ_r^{OH} obtained at the lower temperatures.

The ξ_r^{OH} values that resulted in densities from 263 to 373 K at 1 atm of pressure that were less than 0.2% from the experimental value³² were selected as the appropriate value of ξ_r^{OH} at that temperature and pressure. The data point from 263 K was taken from the work of Hare.³³ Figure 4 shows the results of the simulations at 1 atm at temperatures between 263 and 373 K, showing the excellent agreement with experiment. The final configurations from these runs were used as the starting configurations for all subsequent NPT , NVT , and NVE runs at the specific temperature.

The ξ_r^{OH} values obtained from comparison to the high-pressure data from 2000 to 6000 atm³⁴ varied by less than 0.5%. Figure 5 shows the results of the simulations using the final ξ_r^{OH} values at five temperatures and several pressures each.

The ξ_r^{OH} values thus calculated from the data generating Figures 4 and 5 were plotted as a function of pressure and temperature and polynomial equations were fitted to the above data. The resultant polynomials could be used to determine the appropriate value of ξ_r^{OH} for any temperature or pressure within the fitted range. The resultant equation in a simplified form is

$$\xi_r^{\text{OH}}(T,P) = \sum_{m=0, n=0}^{m=3, n=5} A_{mn} \cdot P^m \cdot T^n \quad (12)$$

where the constant matrix $A(4,6)$ is given in Table 1d and e.

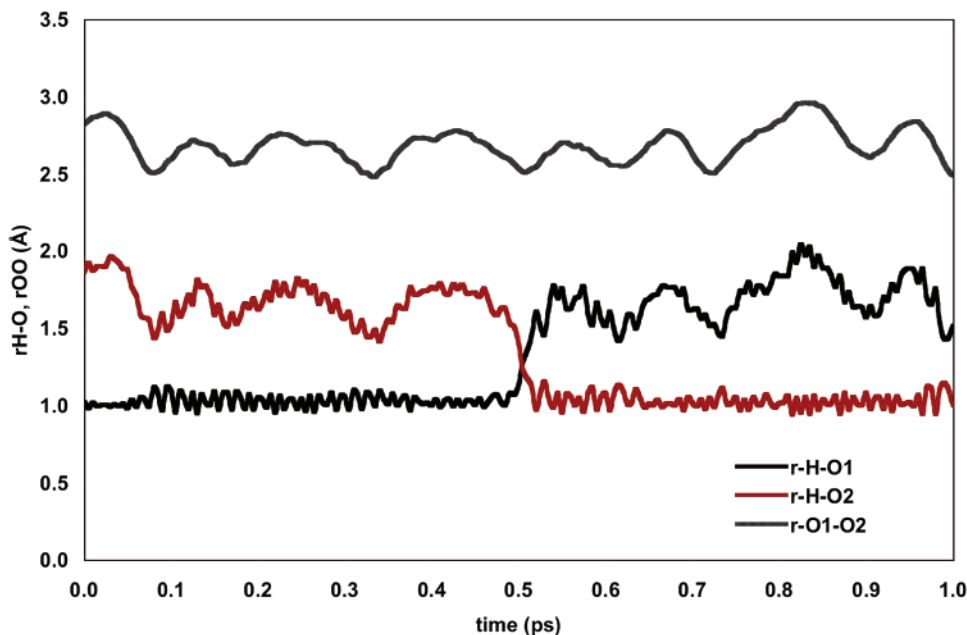


Figure 13. Variation in the HO distances for the reacting H of a hydronium ion during the H exchange with an adjacent water molecule. O1 is the oxygen in the starting H_3O^+ ion, and O2 is the oxygen in the interacting H_2O . At ~ 0.5 ps, the H_3O^+ ion is centered on the O2 oxygen. The O1–O2 separation distance during the reaction is also given, with large oscillations between 2.5 and 3.0 Å.

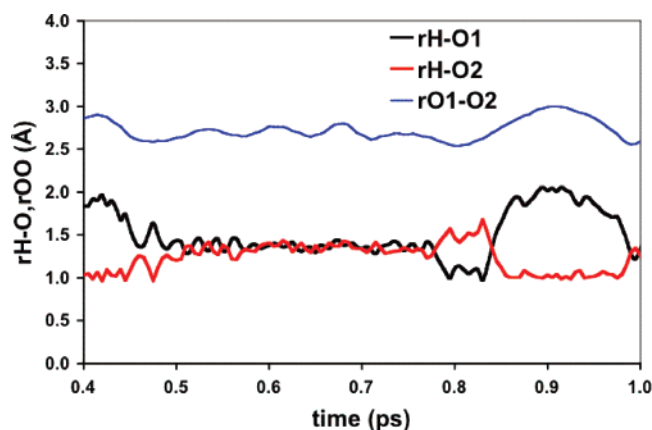


Figure 14. Additional example of hydronium exchange mechanism, where the exchanging H ion sits between both Os, equidistant from each, from ~ 0.5 to ~ 0.75 ps, in this case returning to the original configuration. This pair continues to interact and does show a stable exchange of the proton at 1.7 ps on this time scale (not shown here).

Other parameters are shown in Table 1. The basis for the calibration in the present case has been adherence to the liquid equation of state (EOS) shown in Figure 4 and the equation of state curves in Figure 5.

Results

Molecular Clusters. Water clusters containing from 2 to 9 molecules were simulated for 500 000 timesteps at 50 K using the final parameters shown in Table 1a–e and the ξ_r^{OH} value obtained at 263 K, followed by a 20 000 move continuation run at 1 K with the same parameters. The 50 K run allowed for sufficient rearrangement of the molecules to sample low energy states, with the 1 K run acting as an energy minimizer. The energies shown in Figure 6 for the clusters are given as the average cohesive energy per molecule. Also shown are data taken from ref 14, involving data from minimizations using five other water potentials (POL5/TZ, POL5/QZ, TIP4P/FQ, TIP5P, and MCDHO), plus data from ab initio calculations. The high and low molecular dynamics (MD) results in the figure are taken

from the highest and lowest values from any of the classical potentials and are used to show the spread in data with different interatomic potentials. The trends are similar, with our simulations showing stronger cohesive energies (which would be consistent with the considerations presented by Guillot and Guissani¹⁵ and our dissociative water potential, as discussed below.)

Bulk Water. For data analysis, bulk water simulations with the correct ξ_r^{OH} values were continued from the standard starting configuration for 1×10^6 steps under *NPT* conditions at 1 atm and five different temperatures. The positions and velocities were saved every 2000th step for subsequent data analysis. The averages for the structure and angles were taken from the final 50% of the runs. Further *NPT* calculations at 1 atm were also used in the calculations of the liquid–vapor coexistence curve. An *NVE* ensemble continued from the standard starting configuration for up to 3×10^6 steps was used for calculation of diffusion coefficients at several temperatures using the correct ξ_r^{OH} values. The vibrational spectrum of water was calculated from the Fourier transform of the velocity autocorrelation function. For evaluating the spectrum, the simulations were continued from the standard starting configuration of bulk water simulation for an *NVE* run of 100 000 timesteps with the correct parameters and densities, followed by a 20 000 step run for analysis of the spectrum. Temperature equilibration was carried out for the initial 10 000 steps of the 20 000 move run, and these initial moves were discarded while calculating the velocity autocorrelation function from the final 10 000 saved configurations.

Figure 7 shows the results of the structure of water through the OO, OH, and HH pair distribution functions (PDFs) at five different temperatures (Figure 7a–c) as well as a direct comparison to Soper's most recent experimental data³⁵ (Figure 7d). As can be seen, the PDFs show variations over the five temperatures. The variations are similar to results that were obtained previously.¹⁵ The results of the PDFs at 298 K are compared to experiment³⁵ in Figure 7d and are similar to the

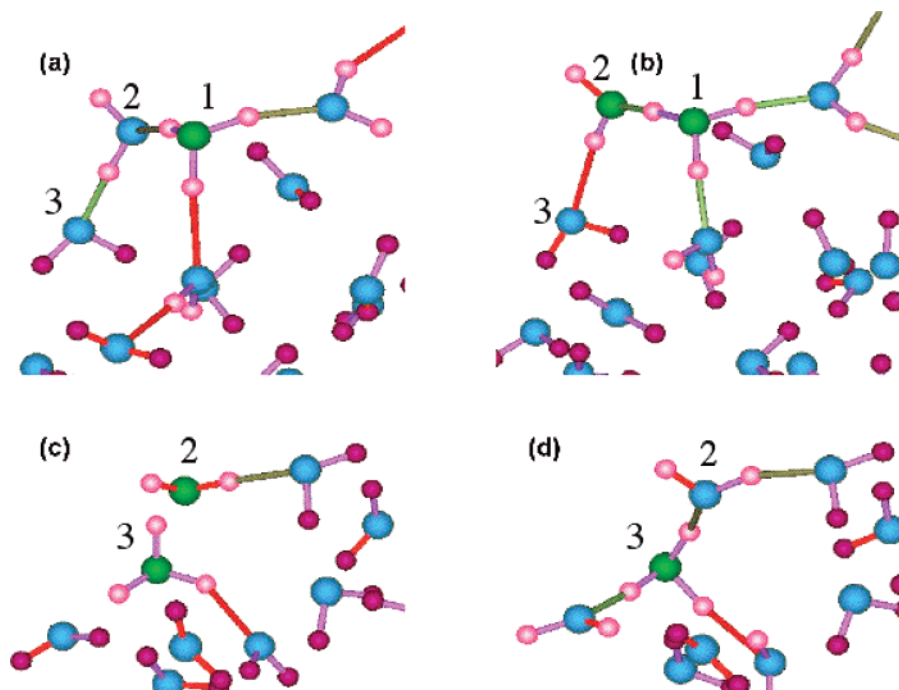


Figure 15. Snapshots of the reaction(s) of the H_3O^+ ion(s) with neighboring water molecules. The color scheme is as follows: green = O in H_3O^+ ion; pink = H attached to O within H_3O^+ ion or in H_2O molecules H-bonded to the H_3O^+ ion; blue = O; small red = H in other waters. The long “bonds” drawn between O–H within 2.0 Å show covalent and H-bonded molecules. The three relevant Os are labeled by numbers 1, 2, and 3. (a) Eigen-type complex with H_3O^+ ion (O1) H-bonded to 3 neighbors. (b) Reacting H ion split between two Os, O1 and O2, with O2 now also marked green. (c) Between frames b and c, a second transfer of a proton occurring to the third water molecule (O3) which forms a Zundel complex. O1 has migrated out of the frame. (d) O3 H_3O^+ now in another Eigen complex.

comparison of several other simulations of water to experiment,¹⁸ although most other simulations do not have the nearest neighbor OH and HH peaks. Clearly, the OH and HH intermolecular pair distributions are precisely equivalent to the experimental data (second and higher peaks). Only the first peaks are too sharp for OH and HH in comparison to experiment, although the locations are accurate. The inset shows an expansion of the OO PDF, with only a slight variance in the depth of the first minimum and maximum in the second peak, although locations are accurate.

Figure 8 shows a comparison between the OO PDF at 298 and 373 K. The main differences are the lowering of the first peak maximum and an increase in the first minimum and slight increase in the location of the second maximum. These results are consistent with previous simulations^{15,21} and experiments³⁵ showing similar shifts in the OO PDF with temperature.

The vibrational spectrum of the simulated bulk water is plotted as a function of temperature in Figure 9. The primary modes of vibration in water at 298 K have been experimentally determined to occur around 400–600, 1600, and 3600–3700 cm^{-1} . The peak near 500 cm^{-1} shifts to lower frequency with increasing temperature, similar to previous work.¹⁵ The most significant effect of changing the temperature is the lowering of the frequencies of the ν_2 mode and a slightly lesser decrease in the stretching mode as well as a broadening of the frequency spectrum in the ν_1 and ν_3 modes. The spectrum at 298 K is similar to the experimental data, except the 1600 peak has shifted upward, probably because of the combined HH repulsion and the HOH 3-body term in the potential function, as also evidenced by the narrow first peaks in the HH and OH PDFs. Nonetheless, the general form is very good in comparison to experiment.

Diffusion coefficients were calculated from the mean square displacement (MSD) of the water molecules in bulk water as a function of temperature. At each temperature, the simulations started from a standard starting configuration and were run for

3×10^6 steps (300 ps) under *NVT* conditions (the correct volume for each *T* was applied for the *NVT* continuations). The MSD was averaged over the final 1.8×10^6 steps. The diffusion coefficients were taken from the average of the slopes of multiple segments of the MSD curve.

Figure 10 shows the resulting values of *D* for several temperatures compared to experimental data.³⁶ The value at 298 K was $2.45 \times 10^{-5} \text{ cm}^2/\text{s}$, which is close to the experimental value of $2.3 \times 10^{-5} \text{ cm}^2/\text{s}$.

The average dipole moment at 298 K was determined to be 2.6 D, consistent with the experimental values that range from 2.3 to 3.2 D.

The cohesive energy of the simulated bulk water at 298 K was calculated as the energy difference between the 1×10^6 steps of the *NPT* run of 392 water molecules at 298 K and an *NVE* run of 500 000 timesteps of 1 isolated molecule of water (the latter without the Wolf sum method). The value obtained was -11.18 kcal/mol , which is the value expected for a simulation with a dissociative water potential. Guillot and Guissani¹⁵ discuss the effect of intramolecular interactions and quantum effects in the intermolecular interactions in the liquid that are not present in rigid water potentials. With an experimental $\Delta H_{\text{vap}}^{\text{exp}}$ of 10.52 kcal/mol,^{15,20} the cohesive energy using the rigid water potential should be -10.4 kcal/mol . However, in our case, changes in the intramolecular interactions between the isolated molecule in the vapor and that in the liquid are taken into account. It is only the intermolecular quantum effects in the liquid that are not included in our simulations. Addition of the intermolecular quantum effects discussed by Guillot and Guissani¹⁵ and the *RT* term would result in a cohesive energy of -11.23 kcal/mol , indicating that our simulation result of -11.18 kcal/mol is very close to the correct value.

In order to test the validity of the potential for reproducing the high-pressure, high-temperature data, an *NPT* simulation of

bulk water at 5000 and 3000 atm was performed at five different temperatures. As anticipated, the variable potential reproduces the experimental density as a function of pressure fairly well, as shown in Figure 11.

The liquid–vapor coexistence curve, shown in Figure 12, was calculated from additional simulations at five higher temperatures, 398, 448, 498, 548, and 598 K starting from the same initial configuration, which had a density of 0.9919×10^{23} atoms/cm³. Runs of 4.0×10^6 moves were made for all the temperatures starting from a 2.2 nm \times 2.2 nm \times 5.0 nm (*xyz*) box of water with 392 water molecules. The simulations included the liquid in contact with a vacuum on either side in the *z* dimension into which the liquid could evaporate. Densities were averaged over 5000 move increments over the last 1.0×10^6 moves and plotted as a function of *z*, from which the density of the liquid was obtained from the hyperbolic tangent function. Results for the liquid at 548 and 598 K showed less than a 4% deviation from the experimental data. Water molecules evaporate into the excess volume at the higher temperatures, although the curve fitting is less accurate for these data because only a few molecules evaporate below 498 K and the excess volume may be a little too low at 598 K, where the vapor is at 0.134 g/cc.

Hydronium Ion Behavior. A cluster of 64 water molecules with one H⁺ ion added was used to evaluate hydronium behavior with this classical potential. The cubic simulation box size was 4.0 nm per side. Two conditions were studied: one where the extra H⁺ ion was placed near an O in a water molecule near the edge of the cluster and a second case where the extra H⁺ ion was placed near an O in a water molecule near the center of the cluster. The former was an *NVE* run of 1×10^6 steps at 298 K with the full coulomb summation, with temperature equilibration for the first 100 000 steps. Within the one million steps, H⁺ ion exchange occurs six times. This implies an average lifetime of ~ 17 ps for the H₃O⁺ ion. Periodic boundary conditions were not used, and all the molecules remained together without the cluster disintegrating. Interestingly, the hydronium ion stays near the periphery of the cluster. In the second case, the *NVE* run was 500 000 steps. Three exchanges occurred in this time frame, giving the same lifetime as the previous run. Also within this time frame in the second run, the hydronium ion migrated (via these exchanges and motion) from the cluster center to the edge of the cluster. Previous studies have similarly seen hydronium migration to the surface.^{24,37} Figure 13 shows the interaction distances between the exchanging H⁺ ion and its two closest O ions (labeled O1 and O2) during a portion of the simulation during which a proton exchange occurred. The 0.0 ps on the time scale is an arbitrary starting point for the figure. Also shown is the O1–O2 distance between the two oxygen ions in the interacting hydronium–water pair, in which O1 is the oxygen in the hydronium ion at the start. The H–O2 distance oscillates as the O2 in the second water molecule approaches the exchanging H⁺ ion. Near 0.5 ps, the exchange occurs rapidly. A different exchange process involving different molecules is observed in Figure 14. In this case, the H⁺ ion is located equidistant between both the O1–O2 oxygen for nearly 0.3 ps. In this particular example, the H⁺ ion returns to its original oxygen but, within ~ 0.7 ps later in this run, exchanges to this same O2. This process of having the H⁺ ion located equidistant between the two interacting Os is consistent with CPMD studies of the hydronium exchange process.²⁷

Figure 15 shows four snapshots of hydronium exchanges observed during a portion of the simulations. Only ions near the hydronium are shown, with some ions looking undercoor-

dated because their attached neighbors are not within the frame of the image. While the H₃O⁺ ion itself may diffuse, additional migration of a H₃O⁺ complex occurs via proton exchanges between a H₃O⁺ ion and neighboring water molecules, as shown in the figure (and previously discussed²⁷). The figure shows the initial H₃O⁺ ion, the O of which is labeled as 1 in part a, which is in an Eigen complex, H₉O₄⁺, changing to more complex structures during proton exchange. Zundel (H₅O₂⁺) and Eigen configurations are observed in the figure and are only two of the multiple configurations occurring in the exchanges.

Conclusions

Molecular dynamics simulations of water were performed using a multibody potential that allows for dissociation of water and varies with environmental conditions. The major variable that changed with the environment was the short-distance OH repulsive term. With small changes in that term alone, the thermal expansion of water at atmospheric pressure and the equation of state at high temperatures and pressures were reproduced. The resultant interatomic multibody potential was then used to simulate other properties. The room-temperature properties of water that were accurately reproduced include the structure, the cohesive energy, the average dipole moment of the liquid, the diffusion constant, the vibrational frequency spectrum, and the transient Eigen and Zundel complexes of the H₃O⁺ ion. In addition, the liquid–vapor coexistence curve was well reproduced.

Acknowledgment. The authors wish to acknowledge funding from the DOE Office of Science, Division of Chemical Sciences, Geosciences, and Biosciences, Grant No. DE-FG02-93ER14385, and from the Division of Material Sciences, Grant No. DE-FG02-97ER45642.

References and Notes

- (1) Rahman, A.; Stillinger, F. H. *J. Chem. Phys.* **1971**, *55*, 3336.
- (2) Rahman, A.; Stillinger, F.; Lemberg, H. *J. Chem. Phys.* **1975**, *63*, 5223.
- (3) Stillinger, F.; Rahman, A. *J. Chem. Phys.* **1978**, *68*, 666.
- (4) Jorgensen, W. L. *J. Am. Chem. Soc.* **1981**, *103*, 335.
- (5) Jorgensen, W. L.; Chandrasekhar, J.; Madura, J. D.; Impey, R. W.; Klein, M. L. *J. Chem. Phys.* **1983**, *83*, 926.
- (6) Weber, T.; Stillinger, F. *J. Phys. Chem.* **1982**, *86*, 1314.
- (7) Jorgensen, W. *J. Chem. Phys.* **1982**, *77*, 4156.
- (8) Zhu, S.-B.; Singh, S.; Robinson, G. W. *J. Chem. Phys.* **1991**, *95*, 2791.
- (9) Sprk, M. *J. Chem. Phys.* **1991**, *95*, 6762.
- (10) Halley, J. W.; Rustad, J. R.; Rahman, A. *J. Chem. Phys.* **1993**, *98*, 4110.
- (11) Rick, S. W.; Stuart, S. J.; Berne, B. J. *J. Chem. Phys.* **1994**, *101*, 6141.
- (12) Dang, L.; Chang, T.-M. *J. Chem. Phys.* **1997**, *106*, 8149.
- (13) Mahoney, M. W.; Jorgensen, W. L. *J. Chem. Phys.* **2000**, *112*, 8910.
- (14) Stern, H. A.; Rittner, F.; Berne, B. J.; Friesner, R. A. *J. Chem. Phys.* **2001**, *115*, 2237.
- (15) Guillot, B.; Guissani, Y. *J. Chem. Phys.* **2001**, *114*, 6720.
- (16) Izvekov, S.; Parrinello, M.; Burnham, C. J.; Voth, G. A. *J. Chem. Phys.* **2004**, *120*, 10896.
- (17) Ren, P.; Ponder, J. W. *J. Phys. Chem. B* **2003**, *107*, 5933.
- (18) Ren, P.; Ponder, J. W. *J. Phys. Chem. B* **2004**, *108*, 13427.
- (19) Robinson, G. W.; Zhu, S.-B.; Singh, S.; Evans, M. W. *Water in Biology, Chemistry, and Physics*; World Scientific: Singapore, 1996.
- (20) Guillot, B. *J. Mol. Liq.* **2002**, *101*, 219.
- (21) Paricaud, P.; Predota, M.; Chialvo, A. A.; Cummings, P. T. *J. Chem. Phys.* **2005**, *122*, 244511.
- (22) Feuston, B. P.; Garofalini, S. H. *J. Appl. Phys.* **1990**, *68*, 4830.
- (23) Lussetti, E.; Pastore, G.; Smargiassi, E. *Chem. Phys. Lett.* **2003**, *381*, 287.
- (24) Dang, L. *J. Chem. Phys.* **2003**, *119*, 6351.
- (25) Zundel, G.; Metzger, H. Z. *Physik. Chem.* **1968**, *58*, 225.
- (26) Eigen, M. *Angew. Chem., Int. Ed. Engl.* **1964**, *3*, 1.
- (27) Marx, D.; Tuckerman, M. E.; Hutter, J.; Parrinello, M. *Nature* **1999**, *397*, 601.

- (28) Wolf, D.; Keblinski, P.; Phillpot, S. R.; Eggebrecht, J. *J. Chem. Phys.* **1999**, *110*, 8254.
- (29) Ma, Y.; Garofalini, S. H. *J. Chem. Phys.* **2005**, *122*, 094508.
- (30) Fennell, C. J.; Gezelter, J. D. *J. Chem. Phys.* **2006**, *124*, 234104.
- (31) Chialvo, A. A.; Cummings, P. T. *Fluid Phase Equilib.* **1998**, *150–151*, 73.
- (32) Wagner, W.; Cooper, J. R.; Dittmann, A.; Kijima, J.; Kretzchmar, H.-J.; Kruse, A.; Mares, R.; Oguchi, K.; Sato, H.; Stocker, I.; Sifner, O.; Takaishi, Y.; Tanishita, I.; Trubenbach, J.; Willkommen, T. *ASME J. Eng. Gas Turbines Power* **2000**, *122*, 150.
- (33) Hare, D. E.; Sorensen, C. M. *J. Chem. Phys.* **1986**, *84*, 5085.
- (34) Kell, G. S. Thermodynamic and Transport Properties of Fluid Water. In *Water-A comprehensive treatise*; Franks, F., Ed.; Plenum press: New York, 1972; Vol. 1.
- (35) Soper, A. K. *Chem. Phys.* **2000**, *258*, 121.
- (36) Mills, R. *J. Phys. Chem.* **1973**, *77*, 685.
- (37) Kusaka, I.; Oxtoby, D. W. *J. Chem. Phys.* **2000**, *113*, 10100.